Swelling of a model polymer network by a one-site solvent: Computer simulation and Flory-Huggins-like theory

Z.-Y. Lu and R. Hentschke
FB Physik, Bergische Universität-Gesamthochschule, D-42097 Wuppertal, Germany
(Received 8 November 2000; published 9 April 2001)

A molecular-dynamics–Widom test particle-simulation was used to investigate the swelling of a model polymer network in contact with a one-site solvent under subcritical and supercritical conditions. Particle motion is computed via molecular dynamics. Simultaneously, the solvent particle concentration is controlled by direct comparison of the chemical potentials in two reference systems (pure solvent and network including solvent), which are calculated using Widom's test particle method. The simulated swelling isotherms exhibit complex behavior: at the subcritical conditions considered here, the swelling ratio decreases with increasing pressure. At the intermediate supercritical temperatures the isotherms exhibit a peak, which disappears with the elevation of temperature. At high temperatures, the swelling ratio of the network increases monotonically with increasing pressure. The corresponding isobars also exhibit a maximum, which broadens and shifts to higher temperatures with increasing supercritical pressure. These results are in qualitative agreement with the prediction of a modified Flory-Huggins theory and with the results of known experiments. Furthermore, the self-diffusion coefficients of the solvent in the network and in its pure state are simulated. The solvent mobility in the network is significantly decreased because of the hindrance of network beads, but exhibits different behavior at subcritical in comparison to supercritical temperatures.

DOI: 10.1103/PhysRevE.63.051801 PACS number(s): 61.25.Hq, 05.10.−a, 05.50.+q, 05.20.−y

I. INTRODUCTION

Computer experiments of polymer networks are motivated by the fact that in contrast to experimental systems the precise control of the network structure is straightforward. Consequently, the relation between swelling behavior and network structure becomes more transparent. Although there are a number of molecular simulation studies on the dynamic and structural properties of polymer networks (see, for example, Refs. [1–3]), detailed studies of their swelling behavior including explicit solvents are scarce. Recently, Escobedo and de Pablo have published Monte Carlo simulations on the swelling of athermal gels [4] and for corresponding gel systems using square well and modified Lennard-Jones potentials [5]. Kenkare *et al.* have conducted combined discontinuous molecular dynamics and Monte Carlo simulations on the swelling behavior of an athermal gel with hard-sphere solvents [6]. Aydt and Hentschke [7] also published results for swelling equilibria in model network-solvents systems with Lennard-Jones nonbonded interactions using Gibbs-Ensemble molecular dynamics simulations [8,9]. To our knowledge, these are the first simulation studies on solvent-network phase equilibria with explicit inclusion of solvent molecules.

Applications of networks are usually confined to subcritical solvent conditions. But with the increasing use of supercritical fluids in experiments where small changes in temperature or pressure may affect the solvent quality of the supercritical fluid significantly [10], the theoretical investigation of network swelling including supercritical as well as subcritical fluids also is of increasing interest. In this paper we use classical molecular dynamics to investigate the swelling of a model network by subcritical and supercritical one-site solvents. During the molecular-dynamics simulations the solvent chemical potentials are calculated via Widom's method [11]. The resulting values in the network simulation cell and in a simulation cell containing only solvent at identical thermodynamic conditions are compared and are used to transfer solvent particles between the simulation cells until chemical equilibrium is attained. Knowing the values of the chemical potentials is useful for understanding the molecular mechanism of the temperature and pressure dependence of the swelling behavior. In particular we discuss the temperature and pressure dependence of the network swelling ratio q, which is in very good qualitatively agreement with an extended Flory-Huggins model. The complex swelling behavior is attributed to the interplay between the excess solvent chemical potentials and the solvent densities in the two simulation boxes. The diffusion of the solvent in the network is also investigated, and the results are found to be in good accord with corresponding experiments.

II. SIMULATION METHOD AND MODEL CONSTRUCTION

In our simulations the particle transfer between a network-solvent box and a pure solvent box is controlled by the direct comparison of their respective solvent chemical potentials, which are calculated via Widom's method [11]. In equilibrium the two boxes, coupled in this fashion, possess the same temperature, pressure, and solvent chemical potential. Such two-boxes–particle-transfer simulations have the advantage that the chemical equilibrium between the bulk phases can be studied without having to include interfaces, which are both time and space consuming. In addition, we have access to the dynamics in the network, because the normal particle translations follow the classical equations of motion. Hereafter we distinguish the two simulation boxes via the indices 0 and 1, and we define a transfer variable ξ

for every solvent particle. $\xi=0$ or $\xi=1$ mean that a particle resides in box 0 or 1, respectively. In our NPT (constant total number of particles, pressure, and temperature) simulation, the chemical potential in the two boxes, $\mu_k(k=0,1)$, can be expressed by [12]

$$\mu_k=\mu_k^i+\mu_k^e, \tag{1}$$

where μ_k^i, the ideal gas chemical potential, is given by

$$\mu_k^i=k_BT\ln\left[\frac{(N_k+1)\Lambda^3}{\langle V_k\rangle}\right] \tag{2}$$

and μ_k^e, the excess chemical potential, can be calculated via the NPT version of the Widom insertion method:

$$\mu_k^e=-k_BT\ln\left[\frac{\langle V_k\exp(-\beta\phi_k)\rangle}{\langle V_k\rangle}\right]. \tag{3}$$

Here $N_k(k=0,1)$ is the number of solvent particles in simulation box k with volume V_k, Λ is the thermal wavelength of the solvent, $\beta=1/k_BT$, where k_B is the Boltzmann constant, T is the temperature, and ϕ_k is the potential energy experienced by the randomly inserted solvent test particle. $\langle\rangle$ in the above equations denotes ensemble averages.

The equations of motion governing the time evolution of our system are

$$\dot{\vec{v}}_i=-\frac{1}{m_i}\frac{\partial\mathcal{U}}{\partial\vec{r}_i}-\zeta_k\vec{v}_i, \tag{4}$$

$$\dot{\vec{r}}_i=\vec{v}_i+\eta_k\vec{r}_i, \tag{5}$$

$$\frac{\dot{L}_k}{L_k}=\eta_k, \tag{6}$$

$$\eta_k=\frac{\kappa_T}{3\tau_P}(P_{\mathrm{inst},k}-P), \tag{7}$$

$$\zeta_k=\frac{1}{2\tau_T}\left(1-\frac{T}{T_{\mathrm{inst},k}}\right), \tag{8}$$

which is the weak coupling method due to Berendsen *et al.* [13]. $\mathcal{U}$ is the total potential energy of the entire system, and $\vec{r}_i$ and $\vec{v}_i$ are the position and the respective velocity of interaction center i with mass m_i. $T_{\mathrm{inst},k}$ and $P_{\mathrm{inst},k}$ are the instantaneous temperatures and pressures, and τ_T and τ_P are the temperature and pressure relaxation times. κ_T is the isothermal compressibility. ${L_k}^3$ is the volume of box k. The equations of motion are integrated via the leap-frog algorithm [14] with an integration step $\Delta t=1.42\times10^{-3}$ in reduced time units.

The total potential energy $\mathcal{U}$ is given by $\mathcal{U}=\mathcal{U}_{LJ}+\mathcal{U}_{\mathrm{net}}$, where

$$\mathcal{U}_{LJ}=\sum_{i<j}4\varepsilon_{ij}\left[\left(\frac{\sigma}{r_{ij}}\right)^{12}-\left(\frac{\sigma}{r_{ij}}\right)^{6}\right]\xi_i\xi_j+\sum_{i'<j'}4\varepsilon_{i'j'}\times\left[\left(\frac{\sigma}{r_{i'j'}}\right)^{12}-\left(\frac{\sigma}{r_{i'j'}}\right)^{6}\right](1-\xi_{i'})(1-\xi_{j'}). \tag{9}$$

The first sum in Eq. (9) describes the nonbonded potential energy in the pure solvent box, where $r_{ij}=|\vec{r}_i-\vec{r}_j|$ is the distance between two solvent particles. The second sum represents the nonbonded potential energy in the box containing both the network and the solvent, where $r_{i'j'}=|\vec{r}_{i'}-\vec{r}_{j'}|$ is the distance between two interaction centers, including solvent-solvent, solvent-network, and network-network (beyond the 1-2 interactions) interaction pairs. To increase the numerical stability during particle transfer without, however, affecting the equilibrium properties of the system, we use a parabolic function $\mathcal{U}_c=-\Sigma_{i<j}[\chi_{ij}(r_{ij}+b)^2+\zeta_{ij}]$, instead of the Lennard-Jones potential whenever r_{ij} is smaller than an inner cutoff radius d. b shifts the vertex of the inverted parabola leading to a nonzero force at $r_{ij}=0$. The parameters χ_{ij} and ζ_{ij} can be evaluated from the conditions $\mathcal{U}_{LJ}(d)=\mathcal{U}_c(d)$ and $d\mathcal{U}_{LJ}(d)/dr_{ij}=d\mathcal{U}_c(d)/dr_{ij}$. Here we use $d/\sigma_{ij}=0.7$ and $b/\sigma_{ij}=0.026$. In addition, we use a long-range cutoff $r_{\mathrm{cut}}=2.9\sigma_{ij}$, beyond which the potential energy is 0. The interactions between bonded network beads $\mathcal{U}_{\mathrm{net}}$ are represented by a harmonic potential

$$\mathcal{U}_{\mathrm{net}}=\sum_{\langle ij\rangle}k_b(l_{ij}-l_0)^2. \tag{10}$$

Here k_b is the force constant, and l_{ij} and l_0 are the actual length and the reference length of the effective bond connecting the network beads i and j. The angular brackets indicate that the summation includes all relevant pairs in the model network. Our model network which is not intended to be a chemically realistic model on the atomic level, is a sixfold coordinated simple cubic lattice with a lattice constant $2l_0$ (see Ref. [7], Fig. 1). Note that we use periodic boundary conditions for the bonded as well as the nonbonded interactions in our system. The corresponding force field parameters together with the thermostat and the barostat coupling constants are compiled in Table I. The parameters for the unlike interaction centers are calculated using the Lorentz-Berthelot mixing rules [14]. Note also that we have tested the dependence of our results on the thermostat and barostat coupling constants, but we did not find any significant effects in a wide range bracketing the values given in Table I.

In order to investigate the swelling of the model network in contact with the one-site solvent, we initially start with 256 nontransferable network beads and 174 solvent particles distributed homogeneously in box 0. Box 1 contains 836 solvent particles. To relax the unfavorable initial network geometry, a 10^5 time steps NVT simulation is executed first without solvent transfer. Subsequently, an NPT simulation is carried out allowing solvent exchange after 10^5 time steps. Typical simulation runs range from 3×10^6 to 6×10^6 time steps total. The solvent exchange between the two simulation

TABLE I. The force field parameters and the thermostat, barostat parameters. The solvent possesses only one center of type *C*. N_N represents the network sites. Note that we have scaled the unit to make $T_c=P_c=m=1$ in our system.

Lennard-Jones	σ	ϵ	m
C	0.457	0.779	1.0
N_N	0.580	0.779	1.0
Bond stretch	k_b	l_0	
N_N-N_N	9083.1	0.722	
	Value		
Δt	1.42×10^{-3}		
τ_T	0.142		
τ_P/κ_T	0.308		

boxes is controlled by direct comparison of the solvent chemical potentials, which are calculated by Eq. (1). This means that during 2×10^3 time steps 5×10^4 test particle positions are generated at random in each of the two boxes, and the excess solvent chemical potential is calculated via Eq. (3). A solvent particle is then transfered by changing its ξ value from 0 to 1 or 1 to 0 attempting to reduce the chemical potential difference. Subsequently this process is repeated.

III. LATTICE THEORY

In order to compare our simulation results with a simple theoretical model, we extend the Flory-Huggins lattice theory [15] by adding empty sites to the system, which is a Sanchez-Lacombe–type proposal [16]. The incorporation of the empty sites is nontrivial and has been considered in other similar theories [5,17] in the context of swelling phenomena. Here we extend a calculation originally presented in Ref. [7] including chainlike solvents as well as the sixfold coordination of our model network in the elastic entropy (and removing an unnecessary assumption). The model is a cubic lattice of $N_0=N_1Q_s+N_2Q+N_3$ sites, where N_1 is the number of solvent chains occupying Q_s neighboring lattice sites, N_2 is the number of network polymer chains occupying Q neighboring lattice sites, and N_3 is the remaining number of empty lattice sites. The free energy F is given by

$$F=U_{\rm conf}-TS_{\rm conf}-TS_{\rm el}, \tag{11}$$

where $U_{\rm conf}$, $S_{\rm conf}$, and $S_{\rm el}$ are the configuration energy, the configuration entropy, and the elastic entropy, respectively. Specifically we have

$$\begin{aligned}F=&\frac{k_BTV}{v_0}[\chi\varphi_1^N\varphi_2-(\chi_1\varphi_1^N+\chi_2\varphi_2)\varphi]\\&+\frac{k_BTV}{v_0}\left[\frac{\varphi_1^N}{Q_s}\ln\frac{\varphi_1^N}{Q_s}+\frac{\varphi_2}{Q}\ln\frac{\varphi_2}{Q}+(1-\varphi)\ln(1-\varphi)\right.\\&\left.-\left(\frac{Q_s-1}{Q_s}\varphi_1^N+\frac{Q-1}{Q}\varphi_2\right)\ln\frac{q_z-1}{e}\right]\\&+\frac{k_BTV}{v_0}\left[\frac{\varphi_2}{Q}\left(\frac{3\alpha^2-3}{2}-\ln\alpha\right)\right].\end{aligned} \tag{12}$$

[Note that $(q_z-1)^{Q+1}$ in Eqs. (16) and (19) of Ref. [7] should be replaced by $(q_z-1)^{-Q+1}$.] Here v_0 is the volume of the unit lattice cell, and V is the total volume of the system. The first term in Eq. (12) is the configuration energy, where $\chi=-q_z(\epsilon_{11}+\epsilon_{22}-2\epsilon_{12})/(2k_BT)$, $\chi_1=-q_z\epsilon_{11}/(2k_BT)$, and $\chi_2=-q_z\epsilon_{22}/(2k_BT)$. q_z is the coordination of the lattice, and ϵ_{11}, ϵ_{22}, and ϵ_{12} are the site-site interaction energies between solvent-solvent, polymer-polymer, and solvent-polymer pairs (note that there are no interaction energies involving empty sites). The solvent volume fraction in the gel φ_1^N is defined as $\varphi_1^N=N_1Q_s/N_0$, and the network polymer volume fraction is $\varphi_2=N_2Q/N_0$. The quantity φ is given by $\varphi=\varphi_1^N+\varphi_2$. The second term is $-T$ times the configuration entropy, and the last term is $-T$ times the elastic entropy of the network. Here $\alpha=(V/V_0)^{1/3}$ is the isotropic one-dimensional deformation ratio of the network. Note that the last term in Eq. (12) is obtained straightforwardly by re-deriving Eq. (21-6) in Ref. [18] using $(\delta V/V)^{2N_2/3}$ for the cubic lattice instead of $(\delta V/V)^{N_2/2}$ for the diamond lattice, where δV is a small volume inside which the crosslinking reaction can occur. Thus, the equation of state for the gel (composed of the polymer network and the solvent) is $P=-(\partial F/\partial V)_{N_0,T}$, i.e.,

$$\begin{aligned}P^*=&\frac{v_0P}{k_BT}\\=&\chi\varphi_1^N\varphi_2-(\chi_1\varphi_1^N+\chi_2\varphi_2)\varphi+\frac{\varphi_1^N}{Q_s}-\ln(1-\varphi)-\varphi\\&-\frac{\varphi_2}{Q}\left(\alpha^2-\frac{4}{3}\right).\end{aligned} \tag{13}$$

Similarly, the free energy and the corresponding equation of state for the pure solvent outside the gel can be written as

$$F=\frac{k_BTV}{v_0}\left[-\chi_1\varphi_1^{S2}+\frac{\varphi_1^S}{Q_s}\ln\frac{\varphi_1^S}{Q_s}+(1-\varphi_1^S)\ln(1-\varphi_1^S)\right], \tag{14}$$

$$P^*=\frac{v_0P}{k_BT}=-\chi_1\varphi_1^{S2}+\left(\frac{1}{Q_s}-1\right)\varphi_1^S-\ln(1-\varphi_1^S), \tag{15}$$

where φ_1^S is the solvent volume fraction. Using that $\alpha=1$ for the dry network, we can write the equation of state in this case as

$$P^*=-\chi_2\varphi_{2,0}^2-\ln(1-\varphi_{2,0})-\varphi_{2,0}+\frac{\varphi_{2,0}}{3Q}, \tag{16}$$

where the subscript 0 refers to the dry network. In equilibrium, the chemical potential of the solvent $\mu_1=(\partial F/\partial N_1)_{V,T}$, should be the same inside and outside the gel. Therefore we obtain

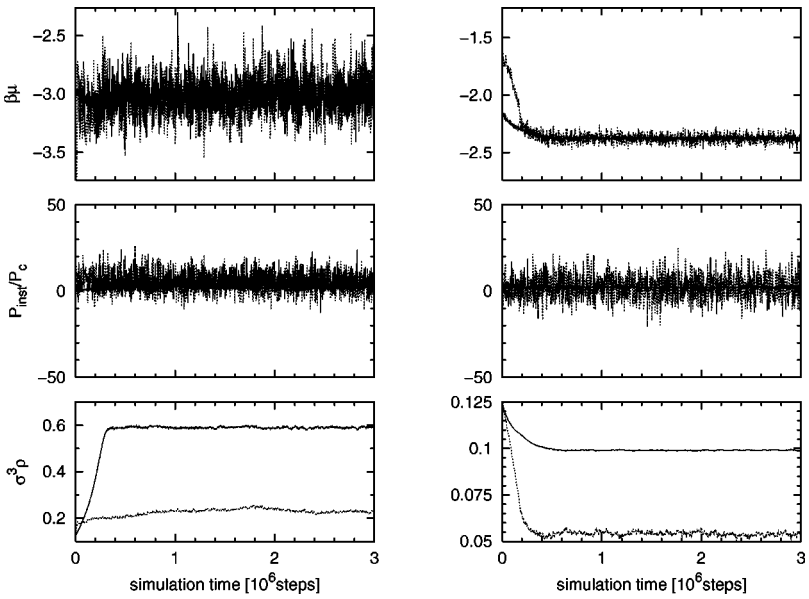

FIG. 1. Time evolution of the reduced solvent chemical potentials ($\beta\mu$), the reduced pressures (P_{inst}/P_c), and the reduced solvent number densities ($\sigma^3\rho$) in the two coupled simulation boxes during runs approaching the equilibrium conditions $T_r=0.89$ and $P_r=2.17$ (left panels) and $T_r=2.10$ and $P_r=2.17$ (right panels). The solid lines represent quantities in the pure solvent box, and the dotted lines represent the same quantities in the network box.

$$(\chi-\chi_1-\chi_2)\varphi_2+2\chi_1(\varphi_1^S-\varphi_1^N)+\frac{1}{Q_s}\ln\frac{\varphi_1^N}{\varphi_1^S}+\ln\frac{1-\varphi_1^S}{1-\varphi}=0. \tag{17}$$

Bearing in mind that the swelling ratio $q=V/V_0=\varphi_{2,0}/\varphi_2$, Eqs. (13), (15), (16), and (17) can be solved numerically for the variables $\varphi_{2,0}$, φ_1^S, φ_1^N, and q. The interaction parameter χ_1 can be obtained via the critical isotherm of Eq. (15), i.e., $\chi_1=2T_c/T$, where T_c is the critical temperature of the pure solvent. For the other two interaction parameters χ and χ_2, we use the expressions $\chi=uT_c/T+v$ and $\chi_2=u_2T_c/T+v_2$, which are subsequently used in this context, where u, v, u_2, and v_2 can be obtained by fitting the simulation results semiquantitatively.

IV. RESULTS AND DISCUSSION

The characteristic quantity describing the swelling of the network is the swelling ratio q. It is defined (see above) as the volume of the swollen network V divided by the volume of the network in a dry reference state V_0 at the same P and T. Here V_0 is obtained via a 10^5 time steps NPT simulation of the dry network with 256 sites. We use several different subcritical and supercritical conditions in the simulations, i.e., $T_r=T/T_c$ takes on the values 0.79, 0.89, 1.05, 1.26, 1.56, 1.84, 1.97, and 2.10, and $P_r=P/P_c$ takes on the values 1.30, 2.17, 4.34, 6.52, 8.69, 10.86, 13.03, and 15.20. Here T_c and P_c are the critical temperature and the critical pressure of the one-site bulk solvent (our units are such that $T_c=P_c=1$).

To illustrate the simulation method, Fig. 1 shows the approach to chemical equilibrium for two selected conditions. The fluctuations of the quantities in the network are large compared to those in the solvent box, but the equilibration of the system is well established. As a check of our chemical potential calculations, Fig. 2 shows the reduced excess solvent chemical potential as a function of reduced number density in the solvent box. Notice that for $T_r=1.84$ the result in this work is in very good agreement with corresponding data from Ref. [19]. The broken lines represent the results obtained via virial expansions including B_3^*, i.e., $\beta\mu^e \approx \sum_{n=1}^{2}(n+1)B_{n+1}^*\rho^{*n}$ [20]. Here B^* is the virial coefficient divided by $b_0=\frac{2}{3}\pi\sigma^3$, and ρ^* is the reduced density. The values of B_2^* and B_3^* are taken from Ref. [21]. It is easily seen that only at very low densities the expansion can be used to predict the excess solvent chemical potential.

Figure 3(a) shows the simulation results for the swelling ratio q as a function of reduced pressure for the various temperatures, i.e., the isotherms. The swelling behavior of the network in contact with the subcritical solvent is strongly

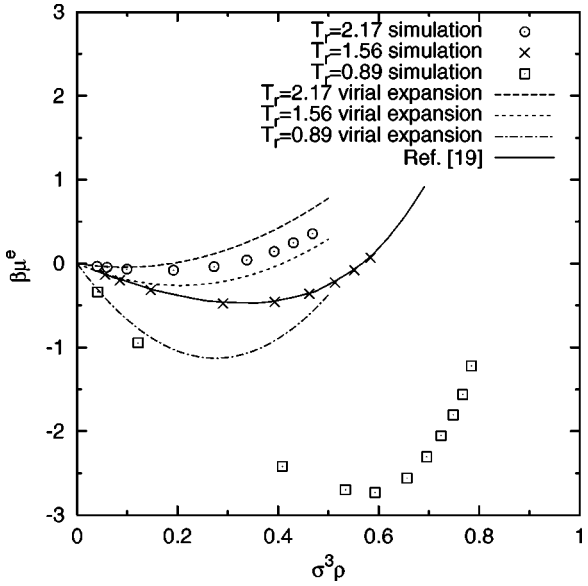

FIG. 2. Reduced excess solvent chemical potential ($\beta\mu^e$) as a function of reduced number density ($\sigma^3\rho$) in the solvent box. The symbols are the results of this work, and the solid line represents a result taken from Ref. [19]. The reduced excess solvent chemical potentials obtained from a virial expansion are shown as broken lines.

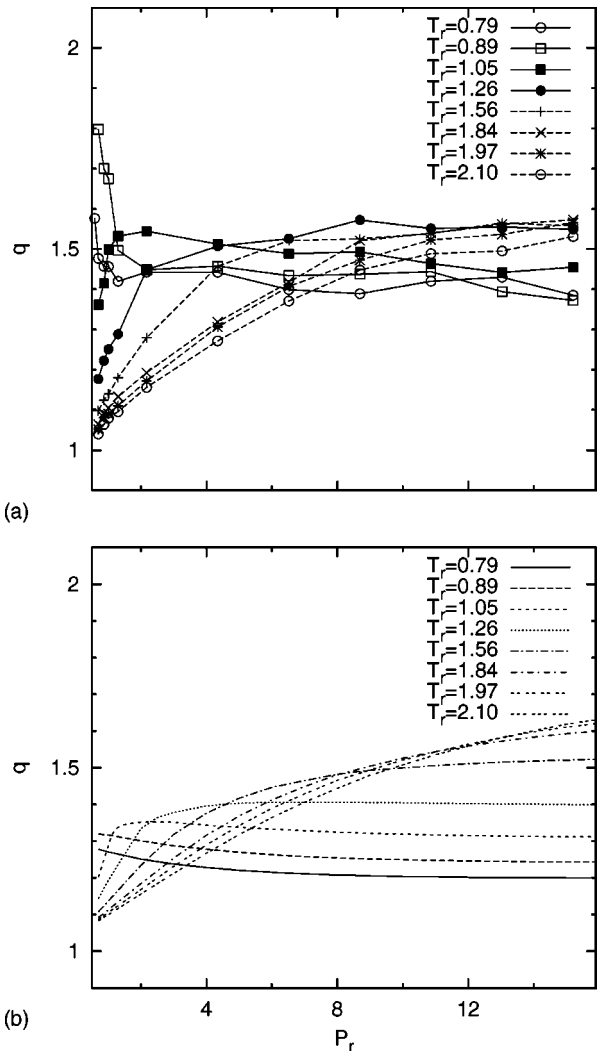

FIG. 3. The simulated q-P_r isotherms. The symbols in (a) are the simulation results, whereas the lines serve to guide the eye. The lines in (b) represent the results of the modified Flory-Huggins theory. Here $\chi=0.7/T_r+0.5$ and $\chi_2=0.2/T_r+2.2$. The parameter values are selected by semiquantatively fitting the isotherm obtained for $T_r=2.1$ in (a).

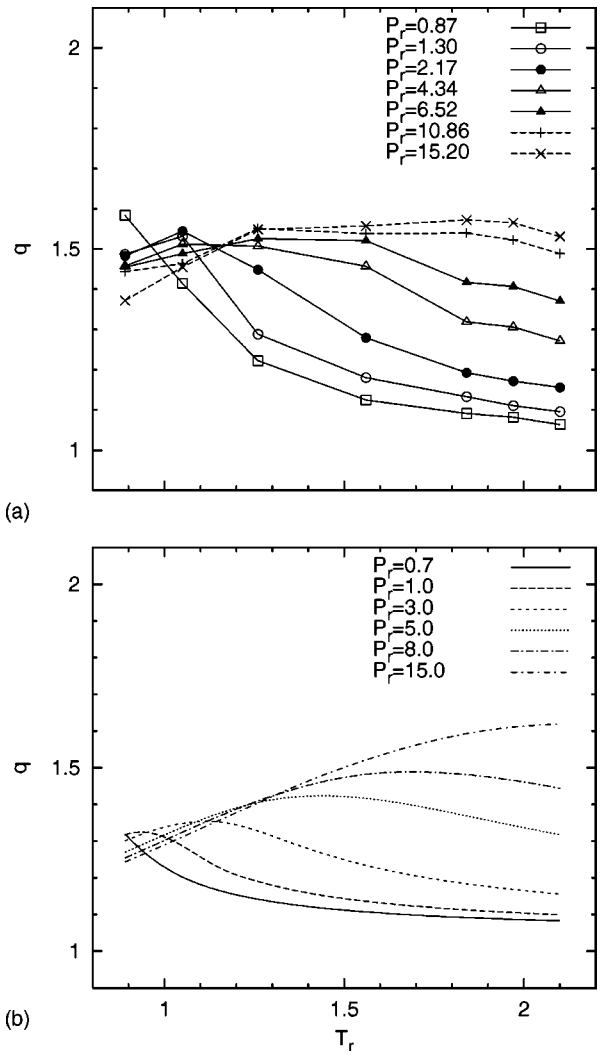

FIG. 4. The swelling ratio (q) as a function of reduced temperature (T_r) for the indicated pressures. The symbols in (a) represent the simulation results, and the lines serve to guide the eye. The lines in (b) are the predictions of the modified Flory-Huggins theory using the same interaction parameters as in Fig. 3(a).

different from that in contact with the supercritical solvent. For $T_r=0.79$ and 0.89, q decreases monotonically with the increase of pressure, while the isotherm exhibits a peak for $T_r=1.05$. Such behavior is also discernible in the curve for $T_r=1.26$, but the peak has moved to a higher reduced pressure. For the higher temperatures ($T_r=1.56$, 1.84, 1.97, and 2.10), q increases monotonically with the increase of the pressure. These differences in the network swelling behavior can be discussed in terms of the difference of the excess solvent chemical potentials in the two simulation boxes (see below). By semiquantitatively reproducing the isotherm at $T_r=2.10$, we obtain the above parameters u, v and u_2, v_2. Slightly different values for these parameters may yield an equally good fit, but this is not important here. Based on these values we may predict the shape of the other isotherms using our modified Flory-Huggins model. As is shown in Fig. 3(b), the theoretical curves are in good qualitative agreement with the corresponding simulation results. In Ref. [5] the authors also show that the swelling of the network is generally greater at higher pressure under supercritical temperatures. A similar tendency can also be found in experiments, for example, for the swelling of silicone rubber by supercritical carbon dioxide [10,22] ($T_r=1.01$, 1.06, and 1.13), the volume of the silicone rubber increases with increasing pressure up to $P_r=4.07$. It should be noted that our result deviates from the corresponding result shown in Fig. 4 of Ref. [7] due to a programming error in the simulation discussed in this reference.

Figure 4(a) shows simulated isobars for six different pressures ranging from subcritical ($P_r=0.87$) to supercritical ($P_r=1.30$, 2.17, 4.34, 6.52, 10.86, and 15.20) conditions. It can be seen that for the subcritical pressure, the isobar monotonically decreases (i.e., the network shrinks) with the increase of the temperature, while under the supercritical pressures, the isobars exhibit a peak. This peak moves to higher

temperature with the increase of pressure and becomes increasingly less pronounced. As is shown in Fig. 4(b), the theoretical predictions for the isobars exhibit the corresponding behavior.

Combining Figs. 3 and 4 we can draw the following conclusions. Under the considered subcritical conditions, the network shrinks with increasing pressure or temperature; at intermediate supercritical conditions q has a maximum, and this maximum shifts to higher supercritical pressures or temperatures with the increase of the corresponding temperature and pressure; at the highest supercritcal pressures and temperatures considered here, the network appears to swell monotonically with the increase of temperature and pressure. This conclusion is in accordance with the results of other theoretical [5,23] and experimental investigations [22,24] in the given subcritical and supercritical conditions.

For a further understanding of the mechanism of network swelling, we can define the solvent site absorbability A as the ratio of the number of absorbed one-site solvents to the number of network beads, i.e., $A=N_{\mathrm{solvent}}/N_{\mathrm{bead}}$. We define this quantity because it reflects the capability of the network to absorb solvent, and it is directly related to the difference of the excess chemical potentials of the solvent in the two boxes. Using Eqs. (1)–(3) we obtain

$$A=\frac{\rho_1 \exp[\beta(\mu_1^e-\mu_0^e)]}{\rho_N}, \tag{18}$$

where ρ_1 is the number density of the solvent in its pure state in equilibrium, ρ_N is the number density of the network beads, μ_0^e and μ_1^e are the excess chemical potentials of solvent in the gel and in the pure solvent, respectively. In Fig. 5(a), the site absorbability A is plotted vs the reduced pressure. Note that A behaves analogous to the swelling ratio shown in Fig. 3(a). The difference of the excess chemical potentials of the solvent between the two simulation boxes $\exp[\beta(\mu_1^e-\mu_0^e)]$ and the density ratio ρ_1/ρ_N are shown in Fig. 5(b) as functions of pressure for two supercritical temperatures ($T_r=1.05$ and 2.10). It can be seen that $\exp[\beta(\mu_1^e-\mu_0^e)]$ always increases with increasing pressure, while the density ratios ρ_1/ρ_N always decreases. Furthermore, at $T_r=1.05$, the pressure has a stronger effect on both the excess chemical potential difference and the density ratio as compared with the $T_r=2.10$ case. As a product of these two quantities, the site absorbability A shows a peak near the critical pressure for $T_r=1.05$, while it increases monotonically with the increase of pressure for $T_r=2.10$. Therefore we draw the conclusion that the competing effects of excess chemical potential and the density ratio during the pressure variation give rise to the observed complex behavior. The site absorbability can also be obtained easily from the modified Flory-Huggins theory via $A=N_1/N_N=\varphi_1^N q/\varphi_{2,0}$ and $\exp[\beta(\mu_1^e-\mu_0^e)]$ can be calculated by rewriting Eq. (17). Figure 6 shows the theoretical site absorbability and $\exp[\beta(\mu_1^e-\mu_0^e)]$ and ρ_1/ρ_N as a function of reduced pressure according to the theoretical prediction. The qualitative agreement between the simulation results in Fig. 5 and the predictions of the modified Flory-Huggins theory is remarkable.

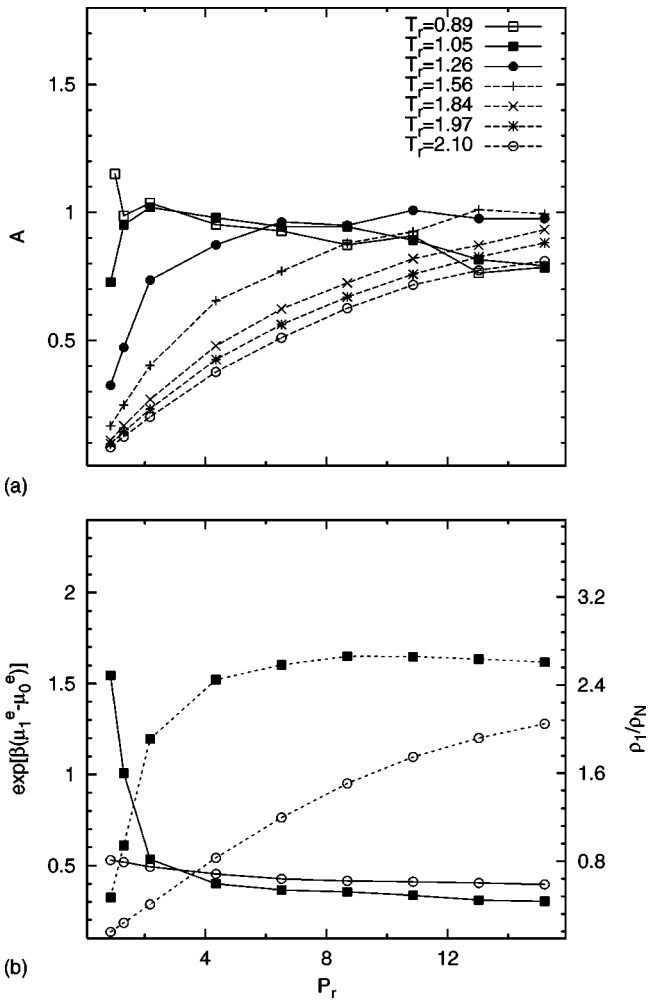

FIG. 5. (a) The site absorbability (A) as a function of reduced pressure (P_r) for different reduced temperatures. (b) $\exp[\beta(\mu_1^e-\mu_0^e)]$ and ρ_1/ρ_N, represented by the solid lines and the dotted lines, respectively, as functions of reduced pressure. The filled squares are the results for $T_r=1.05$, and the hollow circles are for $T_r=2.10$.

One advantage of molecular dynamics simulations in comparison to corresponding Monte Carlo simulations is that the self-diffusion coefficient D can be calculated, for instance, via the Einstein relation

$$D_\alpha=\lim_{t\to\infty}\frac{\langle|r_\alpha(t)-r_\alpha(0)|^2\rangle}{2t}, \tag{19}$$

where $\alpha=x,y,z$, and $D=1/3(D_x+D_y+D_z)$. We show the self-diffusion coefficient of the solvent in the gel D_N and in the bulk solvent D_S as functions of reduced pressure in Figs. 7(a) and 7(b), respectively. Note that Fig. 7(c) also shows the ratio D_N/D_S as a function of reduced pressure. At any of the indicated temperatures, the diffusion coefficients basically decrease with the increase of pressure, and in general, they are much higher at elevated temperatures for constant pressure. Moreover, as shown in Fig. 7(b), the values of D_S under supercritical conditions are on the order of 10^{-4}–10^{-3} $\mathrm{cm^2\,s^{-1}}$, which is approximately 10 times

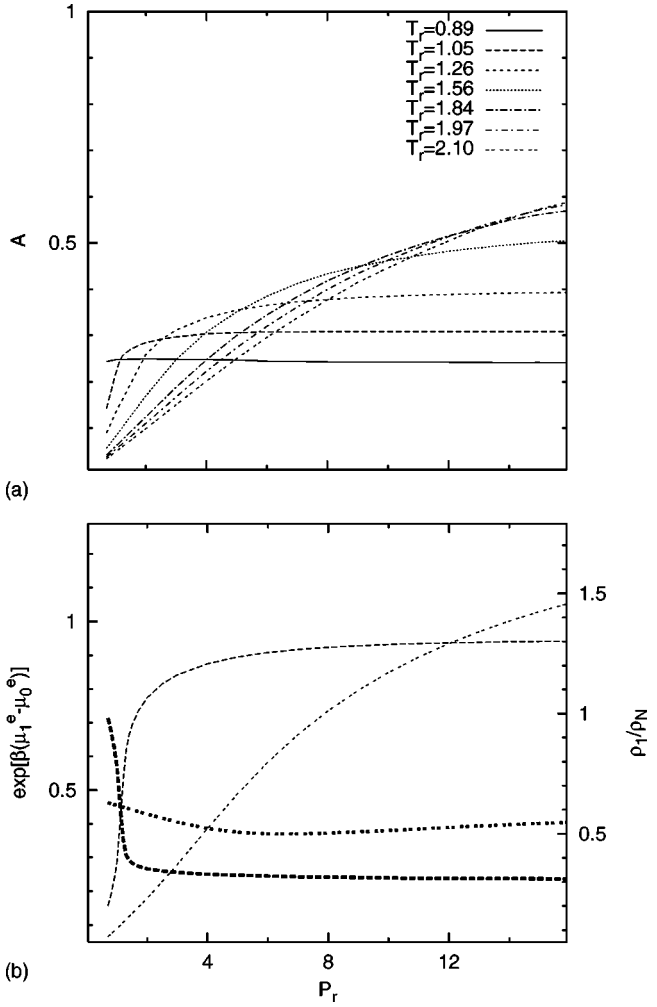

FIG. 6. (a) The results of the modified Flory-Huggins theory for the site absorbability (A) as a function of reduced pressure (P_r) for different reduced temperatures (T_r). (b) $\exp[\beta(\mu_1^e-\mu_0^e)]$ and ρ_1/ρ_N, represented by the bold lines and the thin lines, respectively, as functions of reduced pressure calculated via the modified Flory-Huggins theory. The long-dashed lines are the results for $T_r=1.05$, and the double-dashed lines are for $T_r=2.10$.

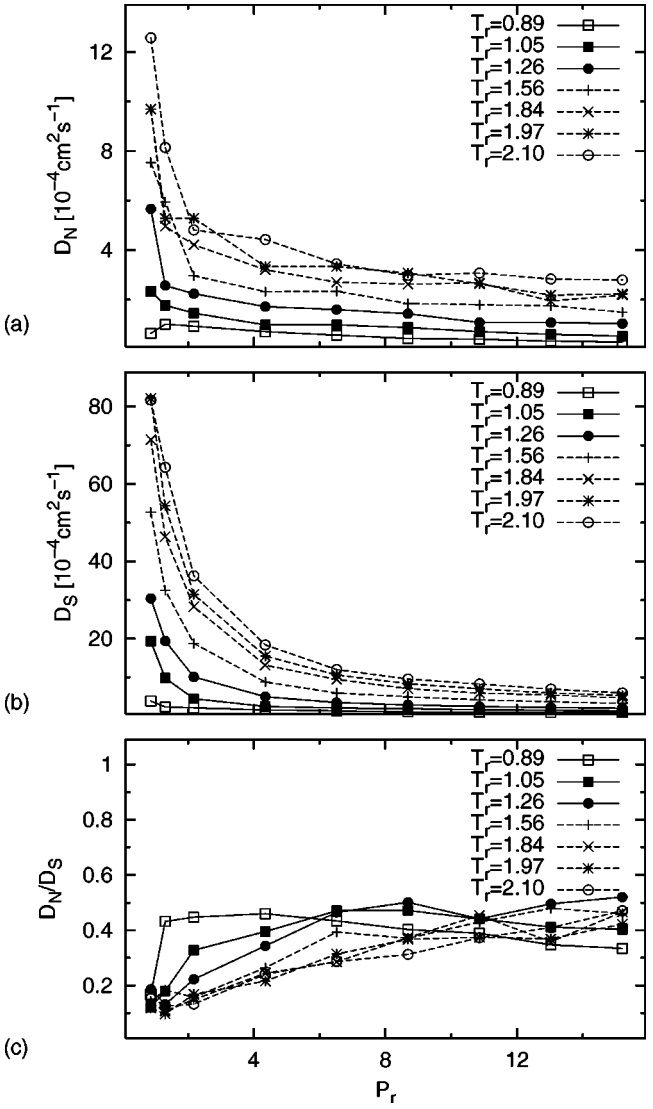

FIG. 7. (a) The self-diffusion coefficients of the solvent in the gel (D_N) as function of reduced pressure. (b) The self-diffusion coefficients of the solvent in its pure state (D_S) as function of reduced pressure. (c) D_N/D_S as function of reduced pressure. The lines are meant to guide the eye.

larger than the corresponding values at the given subcritical condition. This type of fast transport of the solvent is crucial in technological applications. Compared to experimental self-diffusion coefficients [25] under supercritical conditions (here we change the units to reproduce $T_c=190.53$ K and $P_c=46.04$ bar for methane using $\epsilon_M=1.235$ kJ/mol and $\sigma_M=3.79$ Å), we find that the values obtained in our simulations (at $P_r=2.17$, 4.34, 6.51, we obtain 18.8, 8.77, 5.94 and 36.2, 18.4, 12.0×10^{-4} $\mathrm{cm^2\,s^{-1}}$ at $T_r=1.56$ and 2.10, respectively) are in very good agreement with those obtained from the experiments (at $P_r=2.39$, 4.56, 6.73, the values are 15.8, 7.70, 5.74, and 31.5, 18.4, 11.8×10^{-4} $\mathrm{cm^2\,s^{-1}}$ at $T_r=1.55$ and 2.12, respectively). As shown in Fig. 7(c), the diffusion of solvent in the network is significantly decreased because of the hindrance of network beads. For supercritical temperatures there appears to be an overall increase of D_N/D_S with increasing pressure. For the subcritical temperature we observe a sudden increase near $P_r=1$ followed by a slow decrease of D_N/D_S with increasing P_r.

V. CONCLUSIONS

In this paper, we investigate the swelling behavior of a model network by absorbing a Lennard-Jones one-site solvent under subcritical and supercritical conditions using a hybrid molecular dynamics-particle insertion simulation technique. We also correct erroneous results obtained for this system in Ref. [7]. In this work, chemical equilibrium is attained via particle transfer controlled by the direct comparison of the solvent chemical potentials in the two simulation boxes. Temperature and pressure changes give rise to complex swelling behavior. Under the considered subcritical condition, the network shrinks with increasing pressure or temperature; under the intermediate supercritical condition,

the swelling ratio exhibits a maximum, and this maximum shifts to higher supercritical pressures or temperatures with the increase of either temperature or pressure; at the highest supercritical pressure and temperature considered here the network basically swells monotonically as temperature or pressure increase. We attribute the complex swelling behavior to the competing effects of the excess solvent chemical potential difference and the density ratio computed for the two boxes. The mobility of the solvent in the gel is, as expected, hindered by the network beads. But this effect depends rather strongly on the different subcritical or supercritical conditions. A modified Flory-Huggins model is also proposed in this work, and the qualitative agreement between the simulations and the theoretical predictions is found to be quite remarkable. For the conditions studied here, our results are in accord with other theoretical investigations and experimental results.

[1] *Monte Carlo and Molecular Dynamics simulations in Polymer Science*, edited by K. Binder (Oxford University Press, Oxford, 1995), Chap. 4, p. 194.

[2] J.U. Sommer, T.A. Vilgis, and G. Heinrich, J. Chem. Phys. **100**, 9181 (1994).

[3] N.R. Kenkare, C.K. Hall, and S.A. Khan, J. Chem. Phys. **110**, 7556 (1999).

[4] F.A. Escobedo and J.J. de Pablo, J. Chem. Phys. **106**, 793 (1997).

[5] F.A. Escobedo and J.J. de Pablo, J. Chem. Phys. **110**, 1290 (1999).

[6] N.R. Kenkare, C.K. Hall, and S.A. Khan, J. Chem. Phys. **113**, 404 (2000).

[7] E.M. Aydt and R. Hentschke, J. Chem. Phys. **112**, 5480 (2000).

[8] M.J. Kotelyanskii and R. Hentschke, Phys. Rev. E **51**, 5116 (1995).

[9] M.J. Kotelyanskii and R. Hentschke, Mol. Simul. **17**, 95 (1996).

[10] *Supercritical Fluid Technology: Theory and Application to Technology Forecasting*, edited by J.J. MacKetta (Dekker, New York, 1996), p. 1.

[11] B. Widom, J. Chem. Phys. **39**, 2802 (1963).

[12] K.S. Shing and S.T. Chung, J. Chem. Phys. **91**, 1674 (1987).

[13] H.J.C. Berendsen, J.P.M. Postma, W.F. van Gunsteren, A. DiNola, and J.R. Haak, J. Chem. Phys. **81**, 3684 (1984).

[14] M.P. Allen and D.J. Tildesley, *Computer Simulations of Liquids* (Oxford Science, Oxford, 1987).

[15] P.J. Flory, *Principles of Polymer Chemistry* (Cornell University Press, Ithaca, 1953).

[16] I. Sanchez and R.H. Lacombe, J. Phys. Chem. **80**, 2568 (1976).

[17] M. Marchetti, S. Prager, and E.L. Cussler, Macromolecules **23**, 1760 (1990).

[18] Terrell L. Hill, *An Introduction to Statistical Thermodynamics* (Dover, New York, 1986), p. 401.

[19] D. Frenkel and B. Smit, *Understanding Molecular Simulation: From Algorithms to Applications* (Academic Press, San Diego, 1996), p. 161.

[20] J.G. Powles, W.A.B. Evans, and N. Quirke, Mol. Phys. **46**, 1347 (1982).

[21] J.O. Hirschfelder, C.F. Curtiss, and R.B. Bird, *Molecular Theory of Gases and Liquids* (Wiley, New York, 1964), p. 1119.

[22] J.-J. Shim and K.P. Johnston, AIChE J. **35**, 1097 (1989).

[23] D.G. Gromov, J.J. de Pablo, G. Luna-Barcenas, I.C. Sanchez, and K.P. Johnston, J. Chem. Phys. **108**, 4647 (1998).

[24] V. Wiesmet, E. Weidner, S. Behme, G. Sadowski, and W. Arlt, J. Supercrit. Fluids **17**, 1 (2000).

[25] A. Greiner-Schmid, S. Wappmann, M. Has, and H.-D. Ludemann, J. Chem. Phys. **94**, 5643 (1991).